As-Received Physical and Mechanical Properties of the Spar Cap of a GE37 Decommissioned Glass FRP Wind Turbine Blade

Ammar A. Alshannaq, S.M.ASCE[1]; John A. Respert[2]; Lawrence C. Bank, Dist.M.ASCE[3]; David W. Scott, M.ASCE[4]; and T. Russell Gentry, Ph.D.[5]

Abstract: E-glass fiber-reinforced polymer (FRP) composite wind turbine blades are nonbiodegradable, and their end-of-life recycling solutions are limited. Research on reusing and repurposing applications, where minimal amounts of refabrication are needed, is being conducted to address this issue. To design new structures from decommissioned blades, their as-received mechanical and physical properties are needed. Even though some long-term property data for FRP composites exist in the literature, very little actual data for the as-received residual properties of decommissioned blades have been reported. The current work is aimed at developing a methodology to obtain as-received material property data for decommissioned wind turbine blades that are being proposed for use as second-life structural components. In this paper, details of the methods used and the test results for the key physical and mechanical properties of glass FRP material specimens extracted from the spar cap of a decommissioned 1.5-MW GE37 wind turbine blade are reported (the blade is from a General Electric 1.5 MW turbine which is known as a GE37 blade), including burnout testing for constituents' weight and volume fractions as well as fiber architecture and tension, compression, and shear testing in the longitudinal and transverse material directions. Comparisons between test results of other investigators and the experimental data obtained show promising strength and stiffness retention levels of the material for different properties. The results show that structural integrity still exists for the tested composite materials and no deterioration, crack propagation, or delamination was observed in the materials due to the cyclic loading levels experienced in their first life. **DOI: 10.1061/(ASCE)MT.1943-5533.0004410.**

Author keywords: Fiber-reinforced polymer (FRP); Second-life applications; Decommissioned wind blades; Fatigued composites.

Introduction

Wind turbines are growing in size for onshore and offshore wind power (IRENA 2019). This poses problems for disposal at the end of their service life because the materials used in the blades (E-glass fiber and small amounts of carbon fiber embedded in polyester, vinyl ester, or epoxy resin) are nonbiodegradable (Veers et al. 2003; Brøndsted et al. 2005). Because the mass of a wind turbine blade grows exponentially with its length, millions of tons of composite materials will need to be disposed of after the blade service life of 20–25 years (Veers et al. 2003; Liu and Barlow 2017; Bank et al. 2021). It is expected that onshore wind turbines in the range of 0.75–2.6 MW will reach their end-of-life (EOL) in the period 2020–2040 (IRENA 2019). This range of power generation will result in many blades currently in service being decommissioned and in need of sustainable second-life applications.

Even though a variety of methods have been proposed in the literature for recycling and reusing wind blades, none of them are commercially viable at this time. Recycling and reuse of fiber-reinforced polymer (FRP) composites can be divided into three main categories: microscopic-scale, aggregate-scale, and element-scale. The microscopic scale is characterized by chemical and thermal processing to extract the fiber and the matrix for recycling in new products; however, a significant reduction in the properties of the recycled glass fibers has been observed (the main constituent in wind blades). Recycled carbon fibers are giving promising results (Job 2013; Oliveux et al. 2015). The aggregate scale is aimed at reusing mechanically reformed (e.g., ground or cut into small pieces) composites as fillers or aggregates in new products; however, large costs and lower mechanical properties have been found to limit these options (Beauson et al. 2014; Yazdanbakhsh and Bank 2014). The element scale involves reusing small or large segments of the wind blades in new element-sized applications; this is otherwise known as repurposing.

Repurposing is the most circular option in that it recycles the largest percentage of the original product and material. It is also the most cost-effective; because cutting, shredding, and grinding to reduce size are much more expensive than cutting alone, which is all that is needed for repurposing. Repurposing options including small-scale, medium-scale, and large-scale applications have been presented by

[1]Graduate Student, School of Civil and Environmental Engineering, Georgia Institute of Technology, 790 Atlantic Dr., Atlanta, GA 30332 (corresponding author). ORCID: https://orcid.org/0000-0002-3455-3784. Email: aalshannaq3@gatech.edu

[2]Undergraduate Student, School of Mechanical Engineering, Georgia Institute of Technology, 801 Ferst Dr., Atlanta, GA 30332. Email: jrespert3@gatech.edu

[3]Research Faculty, School of Architecture, Georgia Institute of Technology, 245 4th St. NW, Atlanta, GA 30332. ORCID: https://orcid.org/0000-0002-4279-4473. Email: larry.bank@design.gatech.edu

[4]Professor and Chair, Dept. of Civil Engineering and Construction, Georgia Southern Univ., P.O. Box 8077, Statesboro, GA 30460. Email: dscott@georgiasouthern.edu

[5]Associate Professor, School of Architecture, Georgia Institute of Technology, 245 4th St. NW, Atlanta, GA 30332. Email: russell.gentry@design.gatech.edu

Note. This manuscript was submitted on September 29, 2021; approved on January 31, 2022; published online on July 22, 2022. Discussion period open until December 22, 2022; separate discussions must be submitted for individual papers. This paper is part of the ***Journal of Materials in Civil Engineering***, © ASCE, ISSN 0899-1561.

various authors, including Goodman (2010), Jensen and Skelton (2018), Bank et al. (2018), Suhail et al. (2019), Alshannaq et al. (2021a, b), André et al. (2020), Joustra et al. (2021), and Anmet/GP Renewables (2021). The results presented in the literature regarding strength and stiffness retention of FRP composites provide further support for proposed end-of-life applications, where it is expected that the previously used wind blade composite material will retain 80%–90% of its original properties (Nijssen 2006; Post et al. 2008; Lian and Yao 2010).

Very little actual data for the as-received residual properties of decommissioned blades have been reported (Sayer et al. 2013; Ahmed et al. 2021). Certification documents suggest the use of test specimens manufactured in a process sufficiently similar to the wind blade's manufacturing process for quality control testing (DNVGL 2015, 2016). Little attention in the literature has been focused on strength and stiffness retention of these composites after several fatigue cycles in their first life.

This paper presents an extensive testing plan of wind turbine blade composites and provides strength allowables for the materials used in the spar cap (the primary load-carrying element of the blade) of a decommissioned 1.5-MW GE37 wind turbine blade used in the field for 11 years. The turbine was replaced by a larger turbine before reaching its end-of-design-life for the purpose of increasing power generation (a process known as repowering). Test results for the as-received strength and stiffness properties of the composite material from the blade in tension, compression, and shear are reported. The difficulties in testing such thick composites and decisions associated with handling, cutting, testing, and analyzing are emphasized.

Experimental Investigation

Materials

The 1.5-MW GE37 wind turbine blade has a length of 37 m and is made of E-glass fiber embedded in an epoxy resin matrix. Cross sections along the wind blade have three major subcomponents: the shell (the skin, which defines the airfoil shape), the spar cap (the primary load-carrying component, which can be envisioned as flanges), and the webs (the supporting component against shear and buckling) [Fig. 1(a)]. Due to the nature of the loads on the wind blade, the spar cap is expected to have the largest fatigue levels and degradation in strength and stiffness and thus is considered first for as-received property testing.

For this testing program, several spar cap blocks were supplied to the authors from a decommissioned wind turbine blade from a wind farm in Langford, Texas [Fig. 1(b)]. The wind turbine blade was removed from service after 11 years. The blocks were cut from the root-transition region as highlighted in Fig. 1(a). This region was selected for the current work to highlight the most complex cutting process for the thickest part of the spar cap in the wind blade where the thickness reaches 50 mm (the thickness can be even greater for other types of wind blades). Also, large levels of stress are expected at this region of the blade.

Specimens Preparation

Cutting of FRP composites has attracted a lot of attention in the last few decades. Improper cutting techniques can create defects. Additionally, a wind blade's complex geometry necessitates more attention, especially when dealing with coupon-sized samples. Thus, cutting methods, locations, and shapes are highlighted here to illustrate how to obtain representative samples of the original wind blade components where edge damage needs to be minimized to reflect the current state of strength and stiffness of the tested material.

The cutting process of wind blade composites requires special tools that will be listed here with their respective handling steps. However, if simpler tools are used with experience, a similar degree of uniformity in the cut samples can be obtained. The process is as follows:

- Use of large mechanical saws to cut large parts of different components (the large parts are in the range of 1–10 m long by the needed width) from the wind turbine blade structure (which can reach more than 100 m in length).
- Separate the web from the spar cap in the large parts (for the current work, these were already separated and were supplied in 2.5-m-long by 0.5-m-wide parts) and using a diamond-tipped circular saw to cut these parts into blocks (here, each block was cut 0.6–0.8 m long and 0.5 m wide).
- Remove any excess materials from the blocks that will prevent the blocks from lying flat on the waterjet cutter. The excess materials (the bonding material between the spar cap and the web) are removed using an electric planer.
- Affix the processed block to a waterjet to cut smaller FRP strips for use in tension, compression, and shear sampling. If needed, the block can be cut into two pieces (left and right from the middle of the spar cap) for proper handling and laying on the waterjet.
- Cut the strips into smaller pieces (coupons) for final testing. In some cases, the specimen (coupon) shape is prepared using a band saw, a table saw, or the waterjet for minimal edge damage. These steps are shown in Fig. 1.

After cutting the wind blade strips, the process continues to cut smaller coupons for tension, compression, and shear testing according to relevant ASTM standards. Each test coupon has its own shape and dimensions and needs proper handling to avoid excessive damage to the coupons.

Burnout Testing

Small rectangular specimens with dimensions given in Table 1 were cut. ASTM standards D2584 (ASTM 2018a) and D3171 (ASTM 2015b) were followed to burn the specimens and determine the mass fractions, volume fractions, and stacking sequences.

The procedure for determining the stacking sequence is completed by destacking the fiber layers of the specimen after the resin has burned away. Attention should be paid toward the orientation of the specimen relative to its original orientation in the wind blade; for the current work, the specimens for burnout were chosen to be rectangular with the longer direction aligned with the longitudinal direction of the wind blade. At least three specimens were tested at each location on the spar cap block.

Tension Testing

For tension testing, ASTM D3039 (ASTM 2017c) specifies the shape to be rectangular. The specimens' dimensions are given in Table 1. These dimensions were used for both longitudinal (along the wind blade reference axis) and transverse specimens (transverse to the reference axis). The width of the specimen was variable due to the nature of the cut specimens (i.e., the total thickness of the spar cap material in the longitudinal direction is the width of the specimen) [Fig. 1(a)]. This is justified by the fact that the spar cap material consists primarily of unidirectional layers with very thin outside $\pm 45°$ layers (which will be discussed subsequently), and therefore a transversely isotropic material can be assumed. This cutting method is preferable to attempting to cut the coupons

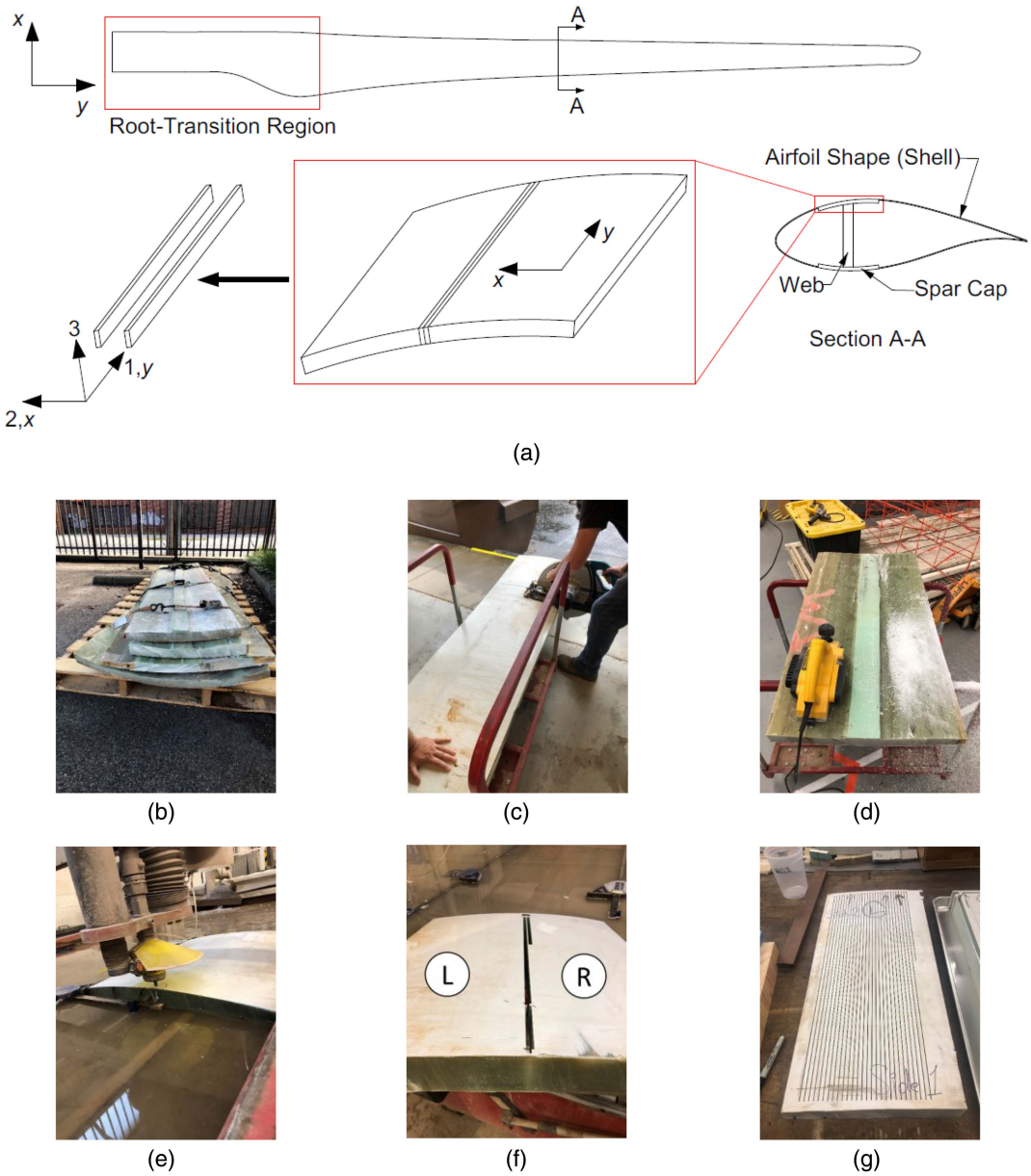

Fig. 1. Cutting of wind blade spar cap samples: (a) location of the cut with a cross section of a single-web wind blade type; (b) large cut parts from the spar cap; (c) initial cutting of a spar cap part into blocks using circular saw; (d) removing the bonding material using electric planer; (e) affixing the block in the waterjet to be cut in two halves (called left and right halves); (f) left and right cutting of the block; and (g) strips cut for mechanical testing.

Table 1. Dimensions of tested specimens

Test type	Dimensions (mm)
Burnout	25.4 × 50.8 mm with the longitudinal direction aligned with the length of the rectangle (to make a reference for fiber direction)
Tension	355.6 mm long × variable width × 6.6 mm thick with gauge length of 203.2 mm
Compression	190.5 mm long × variable width × 6.6 mm thick with gauge length of 38.1 mm
Open-hole tension	304.8 mm long × 38.1 mm width × 6.6 mm thick with gauge length of 152.4 mm
V-notch shear	76.2 mm long × 11.4 mm width measured in the notch region × 6.6 mm thick. The width of the specimen is 19.1 mm for the regions outside the v-notch
Short-beam shear	38.1 mm long × 12.7 mm width × 6.6 mm thick

Note: Some of the specimens have variable width because the width of the specimen is the total thickness of the spar cap material.

horizontally from the curved spar cap. These specimens were tested to determine the tensile strength and elastic modulus of the wind blade composites. The modulus values were calculated in a strain range of 1,000–3,000 $\mu\varepsilon$. A total of 53 specimens were tested in the longitudinal direction, and 13 specimens were tested in the transverse direction. Additionally, 52 specimens in the longitudinal direction and 12 specimens in the transverse direction were used to calculate the elastic modulus.

Compression Testing

For compression testing, different ASTM standards exist, namely D695 (ASTM 2015a), D3410 (ASTM 2016b), and D6641 (ASTM 2016a). ASTM D695 is based on the concept of end bearing (i.e., application of the load through bearing of the specimens' ends on the testing machine platens). ASTM D3410 is based on shear loading (i.e., applying an adequate gripping pressure with rough-surfaced grips, which will transfer longitudinal shear forces to crush the specimen longitudinally in compression). ASTM D6641 is a combined case in which the load is applied through both shear and end bearing on the specimen. Much debate can be found in the literature regarding the best method for testing of thick FRP samples in compression (Camponeschi 1991; Hsiao et al. 1995; Xie and Adams 1996; Daniel and Hsiao 1999). However, after some preliminary testing and a review of the pros and cons of these different methods, ASTM D3410 was chosen for the current testing–especially because these specimens were cut to the required thickness by a waterjet. However, if thicker specimens are to be tested, it is suggested to follow ASTM D6641 to distribute the applied load between shear and end bearing and suppress premature failure of the specimen's ends.

The specimens were rectangular with dimensions in accordance with ASTM D3410, as given in Table 1. These dimensions were used for both longitudinal and transverse specimens. The specimens were tested to determine both the compressive strength and elastic modulus of the material. The modulus values were calculated in a strain range of 1,000–3,000 $\mu\varepsilon$. A total of 73 specimens were tested in the longitudinal direction, and 11 specimens were tested in the transverse direction; five specimens in the longitudinal direction were used to calculate the elastic modulus.

Open-Hole Tension Testing

Open-hole testing is essential in characterizing the behavior of wind blade composites when the second-life applications involve drilling holes and connecting to the spar cap with bolts because these materials were not originally intended for proposed applications where bolting is necessary to connect various components (e.g., crossarms and davits in a power pole application). For open-hole tension tests, ASTM D5766 (ASTM 2018b) was used. The recommended specimens had a rectangular shape with dimensions as detailed in Table 1. These dimensions were used for both longitudinal and transverse specimens. However, the diameter of the notch (i.e., hole) was fixed at 6.35 mm for the longitudinal specimens, leaving a fixed width-to-diameter ratio of 6 and a diameter-to-thickness ratio of 0.96.

For the transverse specimens, the diameter of the notch was variable at 6.35, 4.76, and 3.97 mm, leaving width-to-diameter ratios of 6, 8, and 9.6, respectively, and diameter-to-thickness ratios of 0.96, 0.72, and 0.6, respectively. This was done to investigate the effect of these ratios on the ultimate strength of notched transverse specimens. The width of the specimen was fixed at 38.1 mm following ASTM D5766. Thus, the full thickness of the spar cap was processed (removing excess layers) to reach this width, which involved removing the $\pm 45°$ layers and some of the 0° layers, leaving a notched unidirectional specimen only. Only strength values were measured for open-hole specimens. A total of 11 specimens were tested in the longitudinal direction, and 16 specimens were tested in the transverse direction.

V-Notch Shear Testing

For v-notch shear testing, ASTM D5379 (ASTM 2019) was used. Specimens had dimensions as listed in Table 1, which were used for both longitudinal and transverse specimens. The nature of the cutting plan (using a waterjet) with the required dimensions resulted in specimens that contained unidirectional (0°) layers only. Also, the cutting plan resulted in unidirectional specimens that are described in D5379 as being taken from the 1–3 plane; thus the measurements are based on properties in the 1–3 direction rather than the 1–2 direction, which is more typical of thin composites. However, because the coupons were cut form the interior unidirectional portion of the spar cap, the material is considered to be transversely isotropic and the properties in the 1–2 and in the 1–3 directions are the same and are the in-plane shear properties [Fig. 1(a) shows the 1, 2, and 3 directions].

Both strength and elastic modulus were measured for v-notch specimens. The shear strength was calculated from ultimate (peak) load over the cross-sectional area. The modulus values were calculated as the slope in a strain range of $2{,}500 - 6{,}500\ \mu\varepsilon$ as per ASTM D5379. A total of 26 specimens were tested in the longitudinal direction, and 10 specimens were tested in the transverse direction; three specimens in the longitudinal direction were used to calculate the elastic modulus.

Short-Beam Shear Testing

Short-beam shear testing was completed according to ASTM D2344 (ASTM 2016c). The specimens had rectangular shapes with dimensions as detailed in Table 1. These dimensions satisfy the requirements of D2344 for a length-to-thickness ratio of 6 and a width-to-thickness ratio of 2. These dimensions were used for longitudinal specimens. Only strength values are measured for short-beam shear specimens. A total of 14 specimens were tested in the longitudinal direction.

Experimental Setup and Instrumentation

Burnout Testing

ASTM D2584 directs the use of a Bunsen flame or an electric muffle furnace at 565°C ± 28°C to ignite the resins in the specimens, whereas ASTM D3171 recommends different resin digestion methods to remove the resin from the specimen and determine the mass and volume fractions (in this instance, procedure *G* was used to burn the specimen in a muffle furnace). Volume fractions were obtained from mass fractions using densities for the fiber reinforcement $\rho_r = 2.60\ \text{g/cm}^3$ and the resin matrix $\rho_m = 1.19\ \text{g/cm}^3$ with the assumption that zero void content was present in the material because these composites were manufactured with the vacuum-assisted resin transfer molding (VARTM) process, which results in minimal void contents.

Tension and Compression Testing

Tests were completed using a 245-kN MTS 810 (MTS Systems, Eden Prairie, Minnesota) testing machine with grips powered by 69-MPa hydraulic grip pressure. A constant crosshead displacement of 1.27 mm/min was used as specified by relevant ASTM standards. Tabbing was unnecessary due to the use of serrated grip wedges, which were sufficient to grip the specimens with superficial damage only. An Epsilon Extensometer model 3542 (Epsilon Technology, Jackson, Wyoming) with a gauge length of 25.4 mm was used for specimens with strain measurements on one face only, and Texas Measurements strain gauges (FLAB-5-11-5LJCT-F, College Station, Texas) with a resistance of 120 Ω were used for bending level checks (strain gauges on both faces) and on compressive specimens (short gauge length). The adhesive material used was J-B Weld instant-setting two-part epoxy (J-B Weld, Sulphur Springs, Texas) with a setting time of 1 min. A National Instruments NI

cDAQ-9178 (Austin, Texas) data acquisition system was used with a LabVIEW version 2018 program to help acquire simultaneous strain and load data for specimens with strain gauges. For other specimens, the data acquisition system integrated with the MTS testing machine was used (specimens with no strain gauges).

Gripping pressure in the range 27.6–34.5 MPa was used for longitudinal specimens because these maintain proper integrity of the specimen while mitigating slippage and premature failure of the specimen. However, for transverse specimens, a gripping pressure of 10.3 MPa was used because transverse specimens were excessively damaged by high gripping pressures.

Shear Testing

The two types of shear tests were performed using a 98-kN MTS 810 testing machine. A constant crosshead displacement of 1.27 mm/min was used as specified by relevant ASTM standards. Texas Measurements three-rossette strain gauges (FRAB-2-11-5LJBT-F, Texas Measurements, College Station, Texas) with a resistance of 120 Ω were used for strain measurements of v-notched specimens (for shear modulus calculations). The adhesive material used for bonding strain gauges and the data acquisition systems are the same as those mentioned for tension and compression testing.

Experimental Results

Burnout Tests

To physically characterize the spar cap material of the 1.5-MW GE37 wind blade, the variation in volume fractions at different locations was determined because these materials have different stacking sequences and different thicknesses at different locations. The spar cap local coordinates are shown in Fig. 2(a) in which the x-axis is coincident with the spar cap width and the y-axis is along the reference (longitudinal) axis of the wind blade. The spar cap was divided into six different locations for burnout specimens as shown in Fig. 2(b). Here, $P_1/B_1/1$ means Part 1, Block 1, Location 1.

Table 2 presents the results from the burnout testing. Mass and volume fractions were determined based on procedures and equations presented in ASTM D2584 and D3171. There were no significant changes in the fiber volume fractions across the spar cap block shown in Fig. 2. However, slightly larger values are expected in the central region where the largest thickness of the mostly unidirectional laminate exists, as indicated in Table 2.

Fig. 3(a) shows the destacked $P_1/B_1/1(3)$ and $P_1/B_1/1(4)$ samples as an example (where the numbers 3 and 4 are the repetitions for the burnout samples). All the tested specimens from the spar cap (from the 1.5-MW GE37 at the root-transition region) had the same stacking sequence of $[(\pm 45)_2/\text{Mat}/0_n/(\pm 45)_2]$, where n represents the number of unidirectional layers [Fig. 3(b)]. The mat layer observed in Fig. 3(a) on the inside (bottom) of the spar cap is only visible for some samples where extra strengthening was required at the shell–spar cap connection and was not considered a fixed layer in the stacking sequence. The major variability in properties of the GE37 spar cap material along the wind blade's reference axis comes from the tapering in the longitudinal (0°) layers. No changes in the outside multidirectional layers along the same line in the longitudinal direction of the wind blade were observed except near the tip, where the thicknesses of different parts were reduced. This was also confirmed at other stations along the wind blade (other than the root-transition region) by visual inspection of the cross sections.

It is expected for the spar cap composites of recently manufactured wind turbine blades to have relatively large fiber volume fractions because these blades were designed for relatively large loads and large fatigue levels and were produced using high-quality VARTM (Brøndsted et al. 2005). The results obtained herein (i.e., $V_f = 50\%$) are comparable to those for the materials tested by Samborsky et al. (2012) (i.e., $V_f = 58\%$) with a relatively similar stacking sequence (i.e., the current stacking sequence is $[(\pm 45)_2/\text{Mat}/0_n/(\pm 45)_2]$ which is mostly unidirectional ($n = 97$ layers if the assumed thickness of 0° layer is 0.4572 mm), whereas Samborsky et al. (2012) tested thick unidirectional specimens with a stacking sequence of $[0_{80}]$).

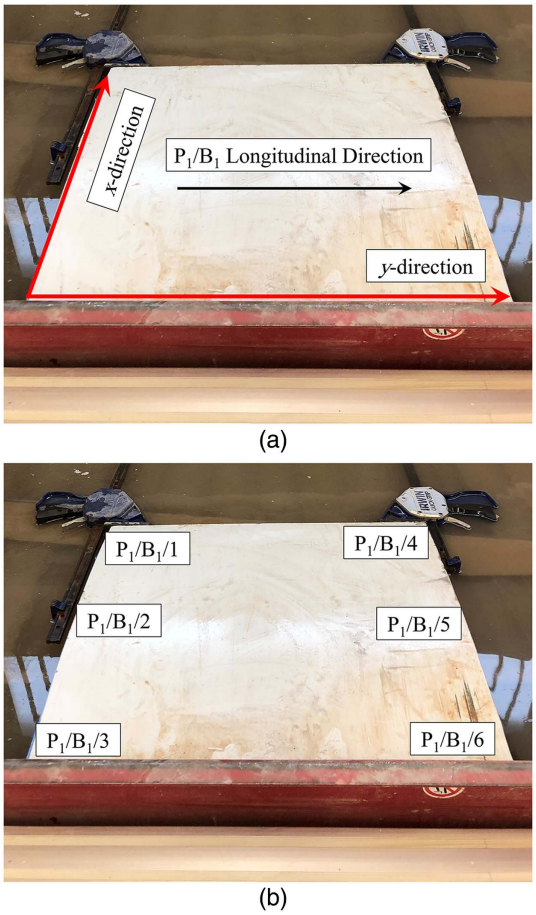

Fig. 2. Spar cap block with (a) defined local coordinates; and (b) locations of burnout specimens.

Summary of All Test Results

Table 3 summarizes the results for various tests conducted in the current study. Some modulus and strain at failure data are not reported because no strain gauging was used.

Tension Tests

Longitudinal Tension

All the tested specimens were equipped with an extensometer on one side. However, five specimens were equipped with strain gauges on both sides as recommended per ASTM D3039. Fig. 4(a) shows a specimen with the installed strain gauges in the testing machine. The strain gauges were applied for two purposes; to check the alignment of the grips (avoiding excessive bending on the tested specimen) and to measure the longitudinal tensile modulus of the composite material (also as a double check on the extensometer

Table 2. Mass and volume fractions of the spar cap for P_1/B_1 samples

Specimen number	M_m [COV (%)]	M_r [COV (%)]	V_m [COV (%)]	V_r [COV (%)]
$P_1/B_1/1$	0.32(0.52)	0.68(0.24)	0.51(0.37)	0.49(0.38)
$P_1/B_1/2$	0.31(0.69)	0.69(0.31)	0.50(0.50)	0.50(0.50)
$P_1/B_1/3$	0.33(1.97)	0.67(0.96)	0.52(1.42)	0.48(1.51)
$P_1/B_1/4$	0.32(0.12)	0.68(0.06)	0.51(0.09)	0.49(0.09)
$P_1/B_1/5$	0.31(0.79)	0.69(0.36)	0.50(0.57)	0.50(0.57)
$P_1/B_1/6$	0.33(4.18)	0.67(2.03)	0.51(3.00)	0.49(3.17)

Note: COV = coefficient of variation; ρ_m = density of epoxy resin matrix = 1.19 g/cm^3; and ρ_r = density of glass fiber = 2.60 g/cm^3.

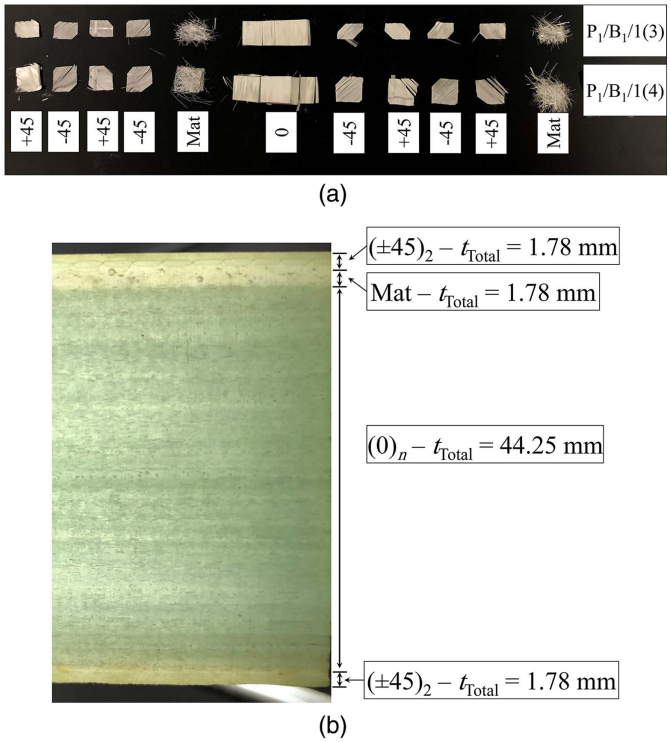

Fig. 3. (a) Stacking sequence of Specimens $P_1/B_1/1(3)$ and $P_1/B_1/1(4)$, with the top to bottom of spar cap from left to right; and (b) thicknesses of layers in a representative specimen having a $[(\pm45)_2/\text{Mat}/0_n/(\pm45)_2]$ stacking sequence.

strain measurement). The limit of bending of the specimen was set to a range of 3% to 5% at moderate strain levels (>1,000 $\mu\varepsilon$) according to ASTM D3039. The stress–strain curve of one of the tested five specimens is shown in Fig. 4(b). As can be seen, small amounts of bending exist (reaching 4.7% at failure), satisfying the requirements of ASTM D3039. Fig. 4(c) shows the mode of failure of the tested specimen. Failure is characterized by a tensile crack in the ±45° layers with multiple longitudinal cracks in the 0° layers. Table 3 summarizes the results of the longitudinal tension tests.

Transverse Tension

The same procedure was used for transverse tension specimens; however, only the extensometer was used. The specimens had some degree of curvature because the spar cap has inherent curvature in the transverse direction. Fig. 5(a) shows the mode of failure of one of the tested specimens, and Fig. 5(b) shows the stress–strain diagram of the specimen. As can be seen from Fig. 5(a), a transverse crack occurred in the gauge length perpendicular to the applied load [the thin line in Fig. 5(a)]. Table 3 summarizes the results of the transverse tension tests.

Compression Tests

Longitudinal Compression

Fig. 6(a) shows a specimen with installed strain gauges on both faces in the testing machine. The limit of bending of the specimen was set to a maximum of 10% up to failure according to ASTM D3410, which recommends a minimum of five specimens to be tested. The stress–strain curve of one of the tested five specimens is shown in Fig. 6(b). As can be seen, small amounts of bending existed (reaching 1.6% at failure), which conforms to the requirements of the ASTM D3410 standard. Small sudden changes in the strain values occurred at ultimate load due to the failure of the specimen. No sudden divergence in strain readings was observed, implying that no global buckling occurred. The mode of failure is shown in Fig. 6(c), which was characterized by inclined cracks initiated at the grip end (due to stress concentrations) and extended through the gauge length. Fig. 6(d) shows the stress–strain curves for all five tested specimens with strain gauges. Table 3 summarizes the longitudinal compression results.

Transverse Compression

The same procedure was used for transverse compression specimens; however, no strain gauging was used. Fig. 7(a) shows the mode of failure of one of the tested specimens, and Fig. 7(b) shows the stress–strain diagram of the specimen. The mode of failure was characterized by an inclined crack driven by shear failure of the resin matrix. This specific mode of failure was also observed by Samborsky et al. (2012) for transverse compression testing of unidirectional specimens and is believed to be due to the pure compression stress state in the specimen, which is transformed into shear stress at 45°, failing the matrix in shear before reaching its compressive strength. Table 3 summarizes the results of transverse compression results.

Open-Hole Tension Tests

Longitudinal Open-Hole Tension

Fig. 8(a) shows the longitudinal open-hole specimen with the extensometer for strain measurements in the testing machine, and Fig. 8(b) shows the stress–strain curve. The extensometer reading was affected by the first crack and the deformation of the hole. Thus, the extensometer reading was eliminated from the stress–strain curve, and no strain data at failure were obtained thereafter. The mode of failure is shown in Fig. 8(c).

As can be seen, the mode of failure of unidirectional notched composites in the longitudinal direction included cracks along the load direction with large deformations of the notch (changing from circular to oval shape). Table 3 summarizes the results of longitudinal open-hole tension tests.

Table 3. Review of experimental results

Property	N	Strength		Modulus		Strain at failure	
		Mean (MPa)	COV (%)	Mean (GPa)	COV (%)	Mean (%)	COV (%)
Longitudinal tension	53	597	9.1	36.8[a]	5.3[a]	1.94[b]	7.8[b]
Transverse tension	13	33.6	11	10.7[c]	4.2[c]	0.29[d]	6.6[d]
Longitudinal compression	74	504	7.9	42.7[e]	6.0[e]	1.22[e]	3.8[e]
Transverse compression	11	114	1.8	—	—	—	—
Longitudinal open-hole tension	11	584	5.1	—	—	—	—
Transverse open-hole tension	16	22.4	10	—	—	0.24	9.0
Longitudinal shear (v-notch)	26	60.8	3.7	4.57[f]	2.7[f]	—	—
Transverse shear (v-notch)	10	27.9	8.9	—	—	—	—
Longitudinal short-beam shear	14	55.0	6.5	—	—	—	—

Note: For transverse compression, transverse v-notch shear, and longitudinal short-beam shear, no strain gauges were used, and thus no modulus or strain at failure data were reported. For longitudinal open-hole tension, extensometer readings were affected by the first crack and the deformation of the hole, and thus no strain at failure data were reported. Also, modulus values have no meaning and thus were not reported. For longitudinal v-notch shear, strain gauges detached before complete failure and thus no strain at failure data were reported; N = number of specimens; and COV = coefficient of variation.
[a]Number of specimens is 52 (47 with extensometer and 5 with strain gauges).
[b]Number of specimens is five (for specimens with strain gauges only).
[c]Number of specimens is 12.
[d]Number of specimens is 9.
[e]Number of specimens is five (for specimens with strain gauges only).
[f]Number of specimens is three (for specimens with strain gauges only).

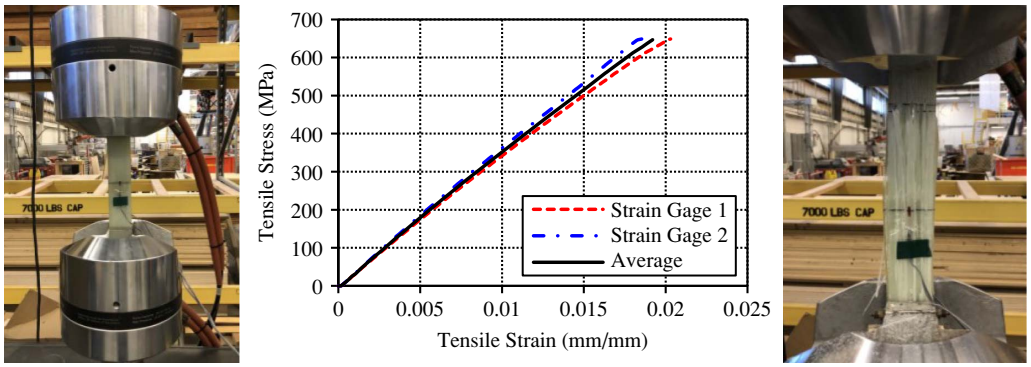

Fig. 4. (a) Specimen in the testing machine; (b) tensile stress–strain diagram; and (c) mode of failure of a representative longitudinal tension specimen.

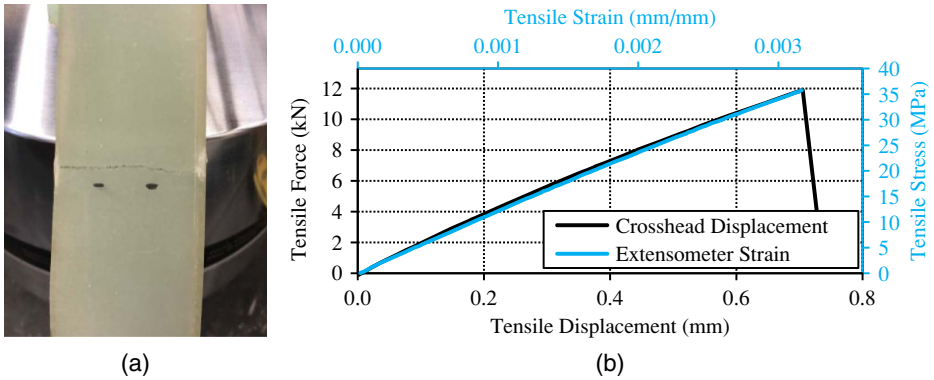

Fig. 5. (a) Mode of failure; and (b) tensile stress–strain diagram of a representative transverse tension specimen.

Transverse Open-Hole Tension

Fig. 9(a) shows the transverse open-hole specimen with extensometer in the testing machine, and Fig. 9(b) shows the stress–strain curve. The mode of failure is shown in Fig. 9(c). As can be seen, the mode of failure of unidirectional notched composites in the transverse direction included a crack across the notch perpendicular to the load direction. Table 3 summarizes the results of transverse open-hole tension tests.

Figs. 10(a and b) show the change in the transverse tensile strength with varying width-to-diameter (w/D) ratios and diameter-to-thickness (D/h) ratios, respectively. The error bars represent ± 1 standard deviation. As can be seen, there were no

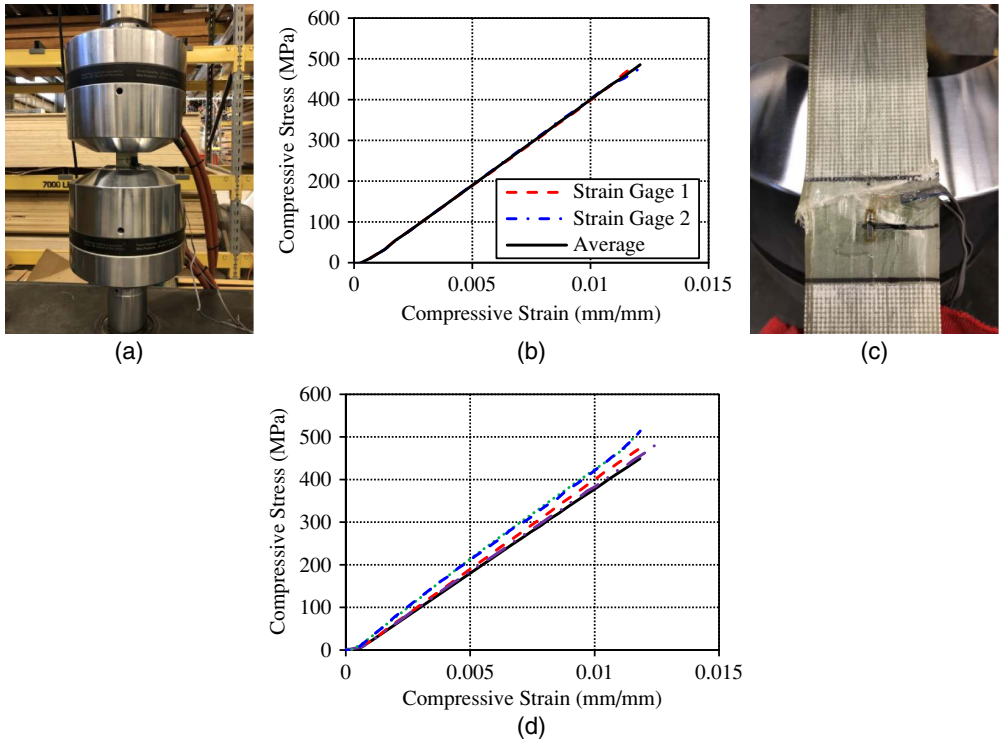

Fig. 6. (a) Specimen in the testing machine; (b) compressive stress–strain diagram highlighting strain readings on both sides of the specimen; (c) mode of failure of a representative longitudinal compression specimen; and (d) compressive stress–strain diagrams of the five specimens with strain gauges.

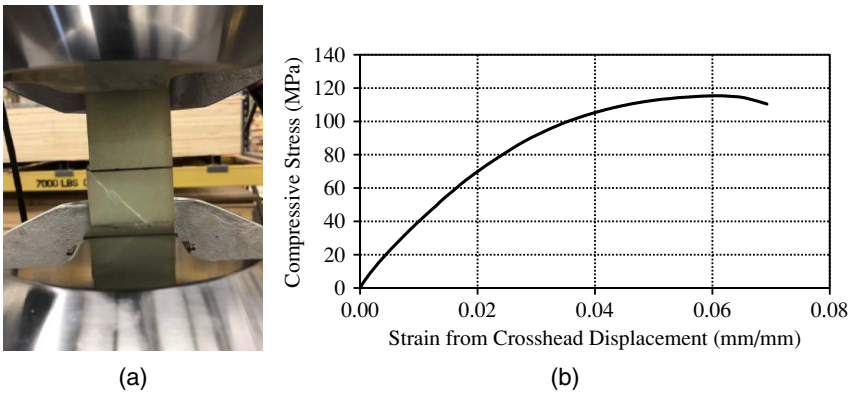

Fig. 7. (a) Mode of failure; and (b) compressive stress–strain diagram of a representative transverse compression specimen.

significant effects of width-to-diameter ratios and diameter-to-thickness ratios on the transverse tensile strength. It is important to mention that ASTM D5766 recommends the use of the gross cross-sectional area of the specimen for stress calculations of open-hole specimens (i.e., disregarding the hole) and thus these charts were constructed based on this recommendation. However, when net area was used, the same observation was confirmed (i.e., no significant effects).

V-Notch Shear Tests

Longitudinal V-Notch Shear

According to ASTM D5379, to determine the in-plane shear modulus of FRP composites, shear strain rosettes need to be installed on the specimen. Fig. 11(a) shows a specimen with an installed shear strain rosette, and Fig. 11(b) shows the mode of failure of the specimen. The mode of failure was characterized by two horizontal cracks at the notch and waving of the 0° layers in the gauge region, abbreviated as the HGN mode in ASTM D5379. The strain gauge was applied to measure the in-plane shear modulus of the spar cap composite. It was assumed that strain gauges on both sides of the specimens were not needed due to expected low levels of twist (ASTM D5379 requires checking twisting levels) because the specimens were cut using a waterjet, which creates specimens with higher quality cutting compared with manual cutting.

The stress–strain curve of one of the tested specimens is shown in Fig. 11(c). As can be seen, nonlinear behavior was observed in the stress–strain curve, as expected for shear properties of

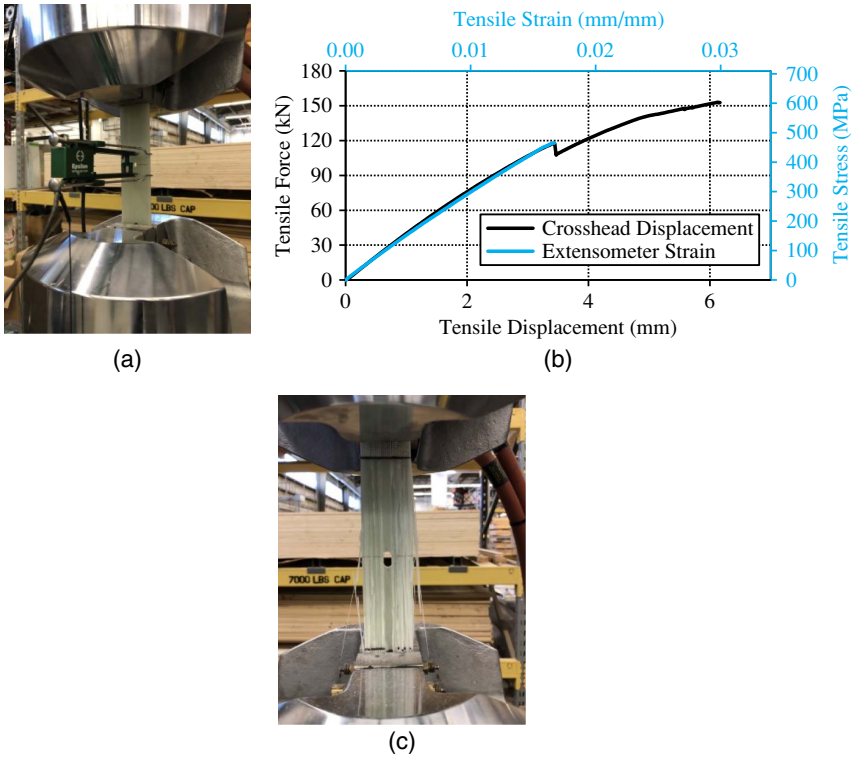

Fig. 8. (a) Specimen in the testing machine; (b) tensile stress–strain diagram; and (c) mode of failure of a representative longitudinal open-hole tension specimen.

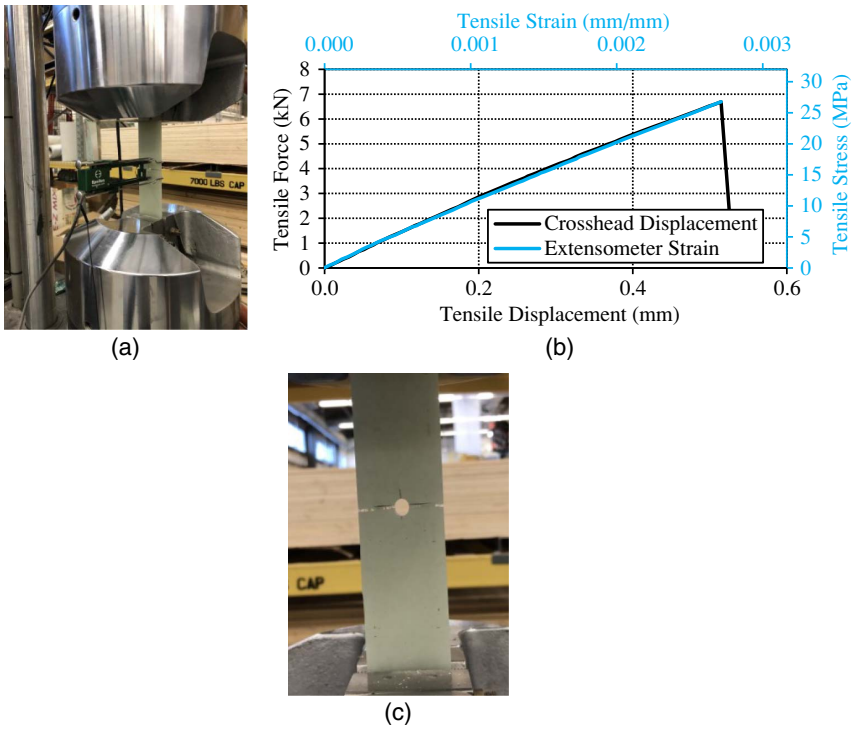

Fig. 9. (a) Specimen in the testing machine; (b) tensile stress–strain diagram; and (c) mode of failure of a representative transverse open-hole tension specimen.

composite materials (El-Hajjar and Haj-Ali 2004). The strain gauge detached from the specimen before complete failure, and thus the figure does not show the full stress–strain curve; however, the data collected were sufficient for modulus calculations, and no strain at failure was measured for any of the specimens tested with strain gauges.

The load-displacement curve of the tested specimen is shown in Fig. 11(d). As can be seen, the first two drops in the load were

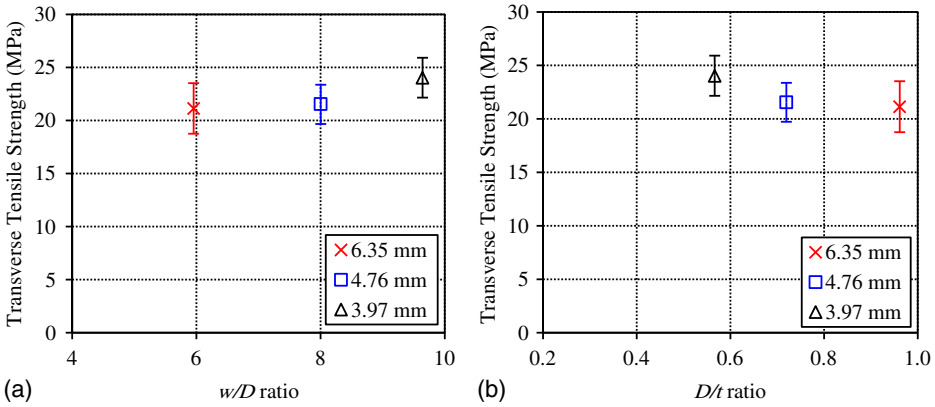

Fig. 10. Effect of (a) width-to-diameter ratio; and (b) diameter-to-thickness ratio on transverse open-hole tensile strength.

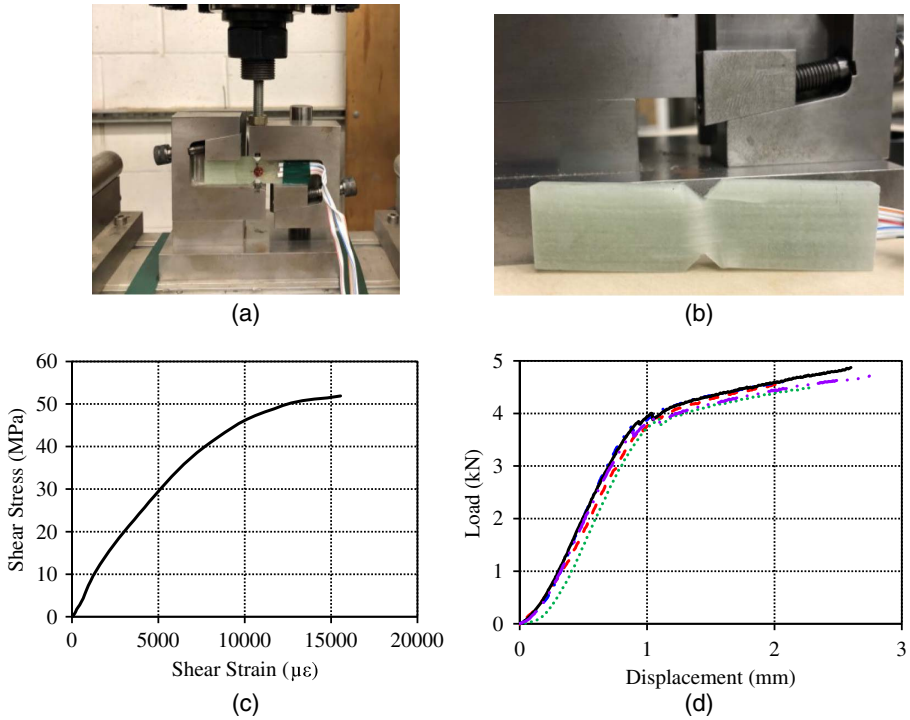

Fig. 11. (a) Installed shear strain rosette; (b) mode of failure; (c) shear stress–strain diagram; and (d) shear load-displacement diagram of representative longitudinal v-notch shear specimens.

linked to the formation of the two horizontal cracks at the notch. Table 3 summarizes the results of the longitudinal v-notch shear tests.

Transverse V-Notch Shear

Fig. 12(a) shows a representative mode of failure, and Fig. 12(b) shows a representative load-displacement diagram of the specimens tested for transverse v-notch shear properties. As can be seen, failure occurred in a sudden drop at ultimate load due to the formation of cracks shown in Fig. 12(a). These cracks are inclined at 45° angles resulting from the state of pure shear, which in turn results in tensile and compressive stresses along the inclined planes, causing eventual failure of the material. Even though this specific mode of failure was not reported in ASTM D5379, the basic mechanics of materials analysis (provided previously) demonstrates that this mode of failure can be considered acceptable. All the tested transverse specimens had this type of failure. Table 3 summarizes the results of the transverse v-notch shear tests.

Longitudinal Short-Beam Shear Tests

Fig. 13(a) shows the specimen in the short-beam shear fixture, and Fig. 13(b) shows the mode of failure of the specimen. This mode of failure was characterized by two interlaminar shear cracks at mid-height of the specimen at the supports where the shear forces were the largest. All the tested longitudinal specimens had this type of failure. Excessive failure underneath the point load was observed; however, the fixture used was based on recommendations from ASTM D2344 for short-beam shear.

Fig. 13(c) shows a representative load-deflection curve for longitudinal short-beam shear. As can be seen, the load-deflection curve continued until the displacement reached 6.6 mm, which

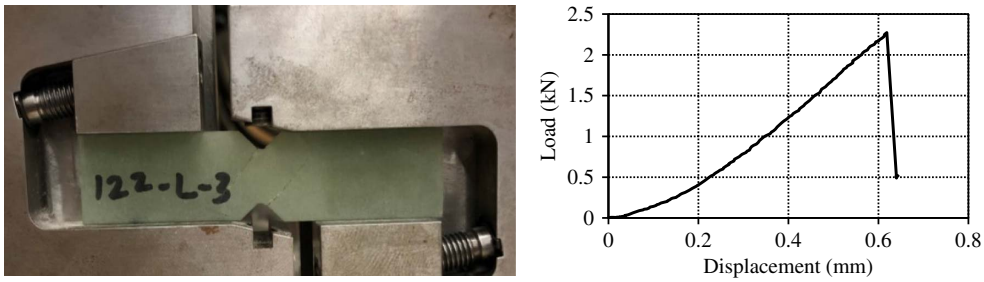

Fig. 12. (a) Mode of failure; and (b) load-displacement curve of a representative transverse v-notch shear specimen.

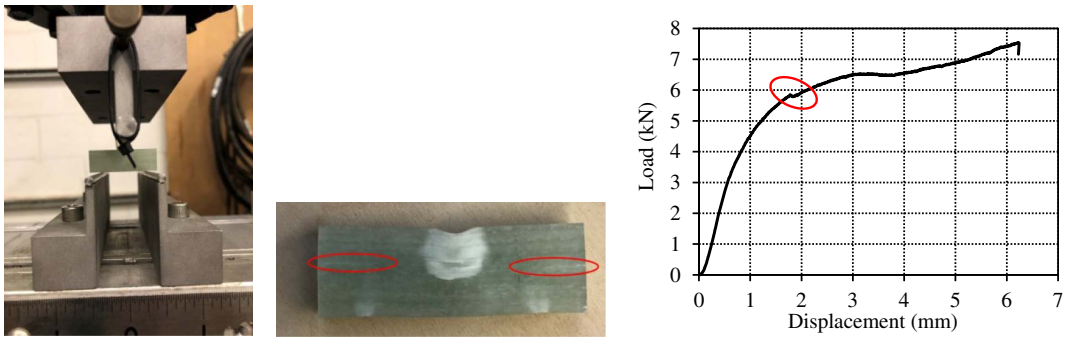

Fig. 13. (a) Specimen in the fixture; (b) mode of failure; and (c) load-displacement curve of a representative longitudinal short-beam shear specimen.

is the specimen's thickness. This is one of the limits that ASTM D2344 specifies to end the test if no drop of 30% in the load is observed. However, in the discussion section of D2344, it emphasized that when the interlaminar shear failure occurs, this is the point to be used for strength calculations (i.e., if interlaminar shear failure is not observed, the results do not represent short-beam shear interlaminar properties), and thus the first drop in the curve [highlighted in Fig. 13(c)] was used for short-beam interlaminar shear strength calculations. Table 3 summarizes the results of the longitudinal short-beam shear tests.

Characteristic Values of As-Received Mechanical Properties for Second-Life Analysis and Design

ASTM D7290 (ASTM 2017a) provides a procedure to determine characteristic values of FRP composites for civil engineering structural applications. The characteristic value is a statistically based material property representing the 80% lower confidence bound on the 5th-percentile value of a specified population; this value accounts for statistical uncertainty for a finite sample size. The characteristic value is intended to determine the materials structural resistance values (i.e., strength allowable) in the design stage. Also, it establishes bases for qualification and acceptance criteria. ASTM D7290 is based on a two-parameter Weibull probability distribution function (Zureick et al. 2006). In some design codes, the characteristic value is taken as mean minus three standard deviations; for example, this is used for FRP bars as concrete reinforcement according to ASTM D7957 (ASTM 2017b). However, the D7290 is considered more statistically valid given its consideration of sample size. The statistical uncertainty originating from the small sample size (a minimum of 10 tests) is accounted for by introducing a data confidence factor.

Table 4 compares the characteristic values obtained from ASTM D7290 with two and three standard deviations from the mean. The characteristic values obtained from ASTM D7290 when compared with the two and three standard deviations from the mean fell mostly between the two values (closer to the lower limit) and in some cases below the lower limit. This gives a reasonable confidence level from the typically used three standard deviations from the mean of the normally distributed data. These characteristic values (obtained at the root-transition region of a 1.5-MW GE37) combined with values obtained at other stations along the wind blade and results from large-scale structural testing (future work by the authors) will form the basis for reliability-based design of structural reuse applications, where reliability indices (β) will be obtained for various limit states and expected failure modes. It is important to mention that the ASCE standard for design of composite structures instructs to use characteristic values for both strength and stiffness in the design process, which will be in future work (ASCE, forthcoming).

Fatigue in Wind Blade Composites

State of As-Received Mechanical Properties of GE37 Material

Table 5 compares the state of the as-received properties of GE37 with data obtained from (1) Sayer et al. (2013) for a 100-kW DEBRA-25 wind blade with a total length of 11.6 m and an 18-year fatigue life with samples taken between 2.0 and 2.4 m from the root,

Table 4. Comparison of the two and three standard deviations from the mean with the characteristic values of the tested materials

Property	$\mu - 2\sigma$ (MPa)	$\mu - 3\sigma$ (MPa)	x_{char} (MPa)	Status of x_{char} relative to $\mu - 2\sigma$ and $\mu - 3\sigma$
Longitudinal tensile strength	488	434	483	Between
Longitudinal tensile modulus	32.9×10^3	30.9×10^3	31.5×10^3	Between
Longitudinal open-hole tensile strength	525	496	511	Between
Transverse tensile strength	29.3	27.7	27.6	Lower
Transverse tensile modulus	9.78×10^3	9.33×10^3	9.51×10^3	Between
Transverse open-hole tensile strength	17.7	15.4	16.3	Between
Longitudinal compressive strength	425	385	427	Upper
Transverse compressive strength	110	108	104	Lower
Longitudinal shear strength (v-notch)	56.2	54.0	54.0	Lower bound
Transverse shear strength (v-notch)	22.9	20.5	20.5	Lower bound
Longitudinal shear strength (SBS)	47.8	44.3	43.2	Lower

Note: μ = sample mean; σ = sample standard deviation; and x_{char} = sample characteristic value.

Table 5. Comparison of as-received mechanical properties of GE37 with data in the literature

Property	Spar cap of GE37	Sayer et al. (2013)[a]	Ahmed et al. (2021)[b]
Longitudinal tensile strength (MPa)	597	477	350
Longitudinal compressive strength (MPa)	504	447	225
Short-beam shear strength (MPa)	55.0	32.3	—
Longitudinal tensile modulus (GPa)	36.8	26.7	15.6
Longitudinal compressive modulus (GPa)	42.7	26.2	—

[a]Data from Sayer et al. (2013).
[b]Data from Ahmed et al. (2021).

and (2) Ahmed et al. (2021) for a 100-kW wind blade with a total length of 9.8 m and age of 20 years (i.e., 14 years in service and 6 years left out of service) with samples taken between 1.6 and 4.6 m from the root. DEBRA-25 was developed in the 1980s by the German Aerospace Research Establishment (DFVLR) with layups ranging between 10 and18 unidirectional layers (0°), 4 and 5 of ±45° layers, and 2 of 0°/90° layers; no specific layup or fiber mass or volume fractions have been reported by Sayer et al. (2013). For the 100-kW wind blade tested by Ahmed et al. (2021), the fiber mass fraction was in the range of 55%–60%, which is equivalent to 38%–43% fiber volume fraction and layups of $[\pm 45/(0/90)_3/\pm 45/\text{Mat}]$, $[\pm 45/(0/90)_3/(\pm 45)_2/\text{Mat}]$, and $[\pm 45/(0/90)_6/(\pm 45)_2/\text{Mat}]$ at 6.6, 4.6, and 1.6 m from the root, respectively.

It can be observed from Table 5 that the results of GE37 provide a promising retention of mechanical properties after the first life of the wind blade. It is important to mention that the GE37 is from newer generation of wind blades that have better production processes compared with those tested by Sayer et al. (2013) and Ahmed et al. (2021) and thus was expected to show better retention of mechanical properties. Table 5 is intended for comparison purposes of the trends expected in fatigued wind blade composites even though these are not for the same power generation level as the GE37 material tested. Other data obtained from the literature (e.g., after Samborsky et al. 2012) were on witness panels which might have not included the influence of manufacturing effects (e.g., ply drops, fiber misalignment, and dry areas) and thus were not compared herein. For example these manufacturing effects are required to be introduced into the test specimens by the certification document DNVGL (2015). Testing composites of the same wind blade tested here (i.e., 1.5-MW GE37) at zero-year life would give a more comprehensive understanding of strength and stiffness retention levels. However, this may not be possible.

It is important to mention that the designs of glass-FRP composite structures are deflection-controlled and that stiffness retention is perhaps more important than strength retention for such designs (Bank 2006; Ascione et al. 2016; ASCE, forthcoming).

Residual Property Data

To get a better idea of the current state of decommissioned wind turbine blades, the experimental results need to be compared with residual strength values after fatigue cycles (i.e., static tests after fatigue). Mandell et al. (2002) and Wahl et al. (2002) presented trends in residual tensile strength after fatigue for $R = 0.1$ and $R = 0.5$ stress ratios. They found that at least 50% was retained after 200,000 cycles. Their data were for a laminate with a stacking sequence of $[90/0/\pm 45/0]_S$, whereas the current program is for a laminate with a stacking sequence of $[(\pm 45)_2/\text{Mat}/0_n/(\pm 45)_2]$. Residual properties testing with the same stacking sequence is scarce in the literature; thus, these results are intended for comparison purposes.

However, Post et al. (2008), Lian and Yao (2010), and Ferdous et al. (2020) emphasized in their analytical, numerical, and experimental studies that only 10%–20% reduction in strength and stiffness values occurred for E-glass FRP composites that gradually degraded over the life span with a sudden drop only at the ultimate stage (i.e., the full capacity of the laminate). However, second-life applications do not necessarily require a detailed prior knowledge of the original state of the wind blade or of its in-service loading history for analysis and design purposes but rather a thorough characterization of the obtained as-received properties (Table 3) and their characteristic values (Table 4).

Conclusions

This paper presented an extensive experimental program for testing composites of a decommissioned wind turbine blade for possible second-life applications. The following findings are emphasized:

- ASTM standards widely used with composites are intended for flat and thin composite specimens; however, the current work deals with thick and curved spar cap specimens. The handling, cutting, and testing procedures were detailed for these complex specimens.
- Promising retention of tensile, compressive, and shear strength and stiffness properties were obtained for these composites when compared with as-received properties of older-generation wind blades.
- Many structural designs of glass FRP composites (e.g., second-life applications proposed for these wind blade materials) are

controlled by serviceability limit states, and the stiffness retention levels observed here are perhaps more important than strength retention for such designs.
- Statistical analysis of the experimental data provides the confidence level in the material properties when ASTM D7290 is followed. The obtained characteristic values are comparable to the common practice of using three-standard deviations from the mean as a measure of nominal material properties.
- The strength and stiffness retentions were obtained for composites from spar cap specimens, where relatively large fatigue levels exist (the spar cap is the primary structural component of the wind blade) and showed promising capability. However, shell and web sandwich materials still need to be addressed in future work for various limit states of sandwich structures.
- The characteristic values obtained in this work for the 1.5-MW GE37 composite wind blade at the root-transition region, combined with future work of obtaining properties for other stations along the wind blade and results from large-scale structural testing, will form the basis for reliability-based design of the proposed second-life applications. Reliability indices (β) will be obtained for various limit states and failure modes.

Data Availability Statement

Some or all data, models, or code that support the findings of this study are available from the corresponding author upon reasonable request.

Acknowledgments

Support for this research was provided by the National Science Foundation (NSF) under Grant Nos. 2016409, 1701413, and 1701694; by InvestNI/Department for the Economy (DfE) under Grant No. 16/US/3334, and by Science Foundation Ireland (SFI) under Grant No. USI-116 as part of the US-Ireland Tripartite research program. The authors would like to thank Logisticus Group for supplying the spar cap specimens for testing and would like to thank Wisconsin Structures and Materials Laboratory at University of Wisconsin-Madison for loaning the Iosipescu fixture for shear v-notch testing.

References

Ahmed, M. M. Z., B. Alzahrani, N. Jouini, M. M. Hessien, and S. Ataya. 2021. "The role of orientation and temperature on the mechanical properties of a 20 years old wind turbine blade GFR composite." *Polymers* 13 (7): 1144. https://doi.org/10.3390/polym13071144.

Alshannaq, A. A., L. C. Bank, D. W. Scott, and R. Gentry. 2021a. "A decommissioned wind blade as a second-life construction material for a transmission pole." *Constr. Mater.* 1 (2): 95–104. https://doi.org/10.3390/constrmater1020007.

Alshannaq, A. A., L. C. Bank, D. W. Scott, and T. R. Gentry. 2021b. "Structural analysis of a wind turbine blade repurposed as an electrical transmission pole." *J. Compos. Constr.* 25 (4): 04021023. https://doi.org/10.1061/(ASCE)CC.1943-5614.0001136.

André, A., J. Kullberg, D. Nygren, C. Mattsson, G. Nedev, and R. Haghani. 2020. "Re-use of wind turbine blade for construction and infrastructure applications." *IOP Conf. Ser.: Mater. Sci. Eng.* 942 (2): 012015. https://doi.org/10.1088/1757-899X/942/1/012015.

Anmet/GP Renewables. 2021. "Anmet installs first recycled wind turbine blade-based pedestrian bridge." Accessed November 17, 2021. https://www.compositesworld.com/news/anmet-installs-first-recycled-wind-turbine-blade-based-pedestrian-bridge.

ASCE. Forthcoming. *Load and resistance factor design (LRFD) for pultruded fiber reinforced polymer (FRP) structures*. Reston, VA: ASCE.

Ascione, L., J.-F. Caron, P. Godonou, K. van IJselmuijden, J. Knippers, T. Mottram, M. Oppe, M. Gantriis Sorensen, J. Taby, and L. Tromp. 2016. *Prospect for new guidance in the design of FRP: Support to the implementation, harmonization and further development of the Eurocodes*. Luxembourg, Europe: Publications Office of the European Union. https://doi.org/10.2788/22306.

ASTM. 2015a. *Standard test method for compressive properties of rigid plastics*. ASTM D695. West Conshohocken, PA: ASTM.

ASTM. 2015b. *Standard test methods for constituent content of composite materials*. ASTM D3171. West Conshohocken, PA: ASTM.

ASTM. 2016a. *Standard test method for compressive properties of polymer matrix composite materials using a combined loading compression (CLC) test fixture*. ASTM D6641. West Conshohocken, PA: ASTM.

ASTM. 2016b. *Standard test method for compressive properties of polymer matrix composite materials with unsupported gage section by shear loading*. ASTM D3410. West Conshohocken, PA: ASTM.

ASTM. 2016c. *Standard test method for short-beam strength of polymer matrix composite materials and their laminates*. ASTM D2344. West Conshohocken, PA: ASTM.

ASTM. 2017a. *Standard practice for evaluating material property characteristic values for polymeric composites for civil engineering structural applications*. ASTM D7290. West Conshohocken, PA: ASTM.

ASTM. 2017b. *Standard specification for solid round glass fiber reinforced polymer bars for concrete reinforcement*. ASTM D7957. West Conshohocken, PA: ASTM.

ASTM. 2017c. *Standard test method for tensile properties of polymer matrix composite materials*. ASTM D3039. West Conshohocken, PA: ASTM.

ASTM. 2018a. *Standard test method for ignition loss of cured reinforced resins*. ASTM D2584. West Conshohocken, PA: ASTM.

ASTM. 2018b. *Standard test method for open-hole tensile strength of polymer matrix composite laminates*. ASTM D5766. West Conshohocken, PA: ASTM.

ASTM. 2019. *Standard test method for shear properties of composite materials by the v-notched beam method*. ASTM D5379. West Conshohocken, PA: ASTM.

Bank, L., E. Delaney, J. Mckinley, R. Gentry, and P. Leahy. 2021. "Defining the landscape for wind blades at the end of service life." Accessed September 1, 2021. https://www.compositesworld.com/articles/defining-the-landscape-for-wind-blades-at-the-end-of-service-life.

Bank, L. C. 2006. *Composites for construction: Structural design with FRP materials*. Hoboken, NJ: Wiley.

Bank, L. C., F. R. Arias, A. Yazdanbakhsh, T. R. Gentry, T. Al-Haddad, J.-F. Chen, and R. Morrow. 2018. "Concepts for reusing composite materials from decommissioned wind turbine blades in affordable housing." *Recycling* 3 (1): 3. https://doi.org/10.3390/recycling3010003.

Beauson, J., H. Lilholt, and P. Brøndsted. 2014. "Recycling solid residues recovered from glass fiber-reinforced composites—A review applied to wind turbine blade materials." *J. Reinf. Plast. Compos.* 33 (16): 1542–1556. https://doi.org/10.1177/0731684414537131.

Brøndsted, P., H. Lilholt, and A. Lystrup. 2005. "Composite materials for wind power turbine blades." *Annu. Rev. Mater. Res.* 35 (1): 505–538. https://doi.org/10.1146/annurev.matsci.35.100303.110641.

Camponeschi, E. T. 1991. "Compression testing of thick-section composite materials." In *Composite materials: Fatigue and fracture*, 439–456. West Conshohocken, PA: ASTM.

Daniel, I. M., and H. M. Hsiao. 1999. "Is there a thickness effect on compressive strength of unnotched composite laminates?" In *Fracture scaling*, 143–158. Berlin: Springer.

DNVGL (Det Norske Veritas Germanischer Lloyd). 2015. "Rotor blades for wind turbines (DNVGL-ST-0376)." Accessed August 9, 2021. https://rules.dnv.com/docs/pdf/DNV/ST/2015-12/DNVGL-ST-0376.pdf.

DNVGL (Det Norske Veritas Germanischer Lloyd). 2016. "Lifetime extension of wind turbines (DNVGL-ST-0262)." Accessed August 9, 2021. https://rules.dnv.com/docs/pdf/DNV/ST/2016-03/DNVGL-ST-0262.pdf.

El-Hajjar, R., and R. Haj-Ali. 2004. "In-plane shear testing of thick-section pultruded FRP composites using a modified Arcan fixture."

Composites, Part B 35 (5): 421–428. https://doi.org/10.1016/j.compositesb.2003.12.004.

Ferdous, W., A. Manalo, J. Peauril, C. Salih, K. Raghava Reddy, P. Yu, P. Schubel, and T. Heyer. 2020. "Testing and modelling the fatigue behaviour of GFRP composites—Effect of stress level, stress concentration and frequency." *Eng. Sci. Technol. Int. J.* 23 (5): 1223–1232. https://doi.org/10.1016/j.jestch.2020.01.001.

Goodman, J. H. 2010. "Architectonic reuse of wind turbine blades." In *Proc., SOLAR 2010 ASES Conf.*, 1–8. Red Hook, NY: Curran Associates.

Hsiao, H. M., I. M. Daniel, and S. C. Wooh. 1995. "A new compression test method for thick composites." *J. Compos. Mater.* 29 (13): 1789–1806. https://doi.org/10.1177/002199839502901307.

IRENA (International Renewable Energy Agency). 2019. "Future of wind—Deployment, investment, technology, grid integration and socio-economic aspects (a global energy transformation paper)." Accessed June 18, 2021. https://www.irena.org/-/media/Files/IRENA/Agency/Publication/2019/Oct/IRENA_Future_of_wind_2019.pdf.

Jensen, J. P., and K. Skelton. 2018. "Wind turbine blade recycling: Experiences, challenges and possibilities in a circular economy." *Renewable Sustainable Energy Rev.* 97 (3): 165–176. https://doi.org/10.1016/j.rser.2018.08.041.

Job, S. 2013. "Recycling glass fibre reinforced composites—History and progress." *Reinf. Plast.* 57 (5): 19–23. https://doi.org/10.1016/S0034-3617(13)70151-6.

Joustra, J., B. Flipsen, and R. Balkenende. 2021. "Structural reuse of high end composite products: A design case study on wind turbine blades." *Resour. Conserv. Recycl.* 167 (2): 105393. https://doi.org/10.1016/j.resconrec.2020.105393.

Lian, W., and W. Yao. 2010. "Fatigue life prediction of composite laminates by FEA simulation method." *Int. J. Fatigue* 32 (1): 123–133. https://doi.org/10.1016/j.ijfatigue.2009.01.015.

Liu, P., and C. Y. Barlow. 2017. "Wind turbine blade waste in 2050." *Waste Manage.* 62 (Sep): 229–240. https://doi.org/10.1016/j.wasman.2017.02.007.

Mandell, J. F., D. D. Samborsky, and D. S. Cairns. 2002. "Fatigue of composite materials and substructures for wind turbine blades." Accessed January 1, 2021. https://pdfs.semanticscholar.org/1c06/d15f077a0c1b96977ea0fc41a68adc31b029.pdf.

Nijssen, R. P. L. 2006. "Fatigue life prediction and strength degradation of wind turbine rotor blade composites." Accessed January 1, 2020. https://energy.sandia.gov/wp-content/gallery/uploads/SAND-2006-7810p.pdf.

Oliveux, G., L. O. Dandy, and G. A. Leeke. 2015. "Current status of recycling of fibre reinforced polymers: Review of technologies, reuse and resulting properties." *Prog. Mater Sci.* 72 (Jul): 61–99. https://doi.org/10.1016/j.pmatsci.2015.01.004.

Post, N. L., S. W. Case, and J. J. Lesko. 2008. "Modeling the variable amplitude fatigue of composite materials: A review and evaluation of the state of the art for spectrum loading." *Int. J. Fatigue* 30 (12): 2064–2086. https://doi.org/10.1016/j.ijfatigue.2008.07.002.

Samborsky, D. D., J. F. Mandell, and P. Agastra. 2012. "3-D static elastic constants and strength properties of a glass/epoxy unidirectional laminate." Accessed January 1, 2020. https://scarab.msu.montana.edu/composites/documents/3D%20Static%20Property%20Report.pdf.

Sayer, F., F. Bürkner, B. Buchholz, M. Strobel, A. M. van Wingerde, H.-G. Busmann, and H. Seifert. 2013. "Influence of a wind turbine service life on the mechanical properties of the material and the blade." *Wind Energy* 16 (2): 163–174. https://doi.org/10.1002/we.536.

Suhail, R., J.-F. Chen, T. R. Gentry, B. Tasistro-Hart, Y. Xue, and L. C. Bank. 2019. "Analysis and design of a pedestrian bridge with decommissioned FRP windblades and concrete." In *Proc., 14th Int. Symp. on Fiber-Reinforced Polymer Reinforcement of Concrete Structures*, 1–5. Belfast, UK: International Institute for FRP in Construction.

Veers, P. S., et al. 2003. "Trends in the design, manufacture and evaluation of wind turbine blades." *Wind Energy* 6 (3): 245–259. https://doi.org/10.1002/we.90.

Wahl, N. K., J. F. Mandell, and D. D. Samborsky. 2002. "Spectrum fatigue lifetime and residual strength for fiberglass laminates." Accessed January 1, 2021. https://prod.sandia.gov/techlib-noauth/access-control.cgi/2002/020546.pdf.

Xie, M., and D. F. Adams. 1996. "Influence of unidirectional composite compression specimen thickness and loading method." *J. Reinf. Plast. Compos.* 15 (12): 1217–1225. https://doi.org/10.1177/073168449601501203.

Yazdanbakhsh, A., and L. C. Bank. 2014. "A critical review of research on reuse of mechanically recycled FRP production and end-of-life waste for construction." *Polymers* 6 (6): 1810–1826. https://doi.org/10.3390/polym6061810.

Zureick, A.-H., R. M. Bennett, and B. R. Ellingwood. 2006. "Statistical characterization of fiber-reinforced polymer composite material properties for structural design." *J. Struct. Eng.* 132 (8): 1320–1327. https://doi.org/10.1061/(ASCE)0733-9445(2006)132:8(1320).